



Journal of Applied and Computational Mechanics



Research Paper

Nonlinear Biodynamic Models of the Hand-arm System and Parameters Identification using the Vibration Transmissibility or the Driving-point Mechanical Impedance

Nahid Hida¹, Mohamed Abid², Faouzi Lakrad³

¹ Laboratory of Renewable Energy and Dynamics of Systems, Faculty of Sciences Ain Chock, University Hassan II of Casablanca, B.P. 5366 Maarif, Casablanca, 20100, Morocco, Email: nahid.hida@gmail.com

² Laboratory of Renewable Energy and Dynamics of Systems, Faculty of Sciences Ain Chock, University Hassan II of Casablanca, B.P. 5366 Maarif, Casablanca, 20100, Morocco, Email: Mohamed.abid@univh2c.ma

³ Laboratory of Renewable Energy and Dynamics of Systems, Faculty of Sciences Ain Chock, University Hassan II of Casablanca, B.P. 5366 Maarif, Casablanca, 20100, Morocco, Email: faouzi.lakrad@univh2c.ma

Received October 22 2020; Revised December 20 2020; Accepted for publication January 13 2021.

Corresponding author: F. Lakrad (faouzi.lakrad@univh2c.ma)

© 2021 Published by Shahid Chamran University of Ahvaz

Abstract. This study aims at deriving nonlinear expressions of the transmissibility and the driving-point mechanical impedance (DPMI) of two nonlinear biodynamic hand-arm models having active restoring and dissipative parameters. It aims also in computing explicitly the non-directly measurable stiffness and damping coefficients of the human hand-arm system (HAS). Multivariate Padé approximants are used to express the dependence of the HAS mechanical properties on various influencing factors. The harmonic balance method is used to derive analytical expressions of the transmissibility and the DPMI. Then, the models parameters are identified by minimizing constrained error functions between the theoretical DPMI or transmissibility and the measured data. The developed workflow is applied to three experimental data sets of Z-direction vibrations where the excitation frequency and/or the grip force are varied. Using the ISO-10068 (2012) limit DPMI values versus the excitation frequency, we derived upper and lower limits of the overall stiffness coefficient and damping ratio for the human HAS. Furthermore, the model reproduces with high accuracy experimental measurements of the transmissibility, the DPMI and the vibration power absorption.

Keywords: Hand-arm vibration, Nonlinear transmissibility, Driving-point mechanical impedance.

1. Introduction

Studying the biodynamic of the hand-arm system (HAS) is a keystone of understanding mechanisms of hand-arm vibration syndromes (HAVS) and developing better standards to prevent them. Moreover, the knowledge of the biodynamic response of the HAS is useful for designing less vibrating hand tools and for developing hand-arm simulators to test them [1, 2]. The experimental characterization of the HAS biodynamic behavior is based on measuring the vibration transmissibility and/or the driving-point mechanical impedance (DPMI). The transmissibility [3, 4] gives information about rates of vibrations at different loci of the HAS. The DPMI describes the mechanical resistance to vibrations and gives information on the overall behavior of the HAS under a specific excitation. It describes also the vibrational absorbing properties of the HAS that can be used to quantify the vibration exposure risk [5, 6]. Many factors influence the measured transmissibility and DPMI, we cite among others the forcing properties, the hand forces, the hand-arm posture, the human anthropometric characteristics and vibration susceptibility [7-9].

The HAS is a very complex system that is composed of a large number of non-homogeneous elements such as bones, muscles, blood vessels, nerves and skin. Due to this structural and material complexity of the HAS, lumped parameters models are widely used in the literature to describe its response to imposed vibrations [3, 10, 11]. These models use linear systems with passive and constant masses, stiffness and viscous damping coefficients regardless of the experimental conditions. Furthermore, their mechanical behaviors are acknowledged to be nonlinear and that the skin-muscle-bone characteristics change with changing experimental conditions.

In a review paper Rakheja et al. [10] investigated the suitability of 12 mechanical single point hand-handle coupling linear models of the HAS, reported in the literature, through their biodynamic responses that are derived from the measured DPMI. These models include mass-spring-damper systems (MSD) of 1 to 4 DOF and models combining beams and MSD. They showed that the DPMI magnitude and phase determined by the single degree of freedom (SDOF) model, with constant parameters, are outside the range of the values recommended in the ISO-10068 (2012) [12], for large frequency intervals. In fact, the SDOF model with constant parameters has only three parameters that are the mass, the stiffness and the damping coefficients. Two strategies can be attempted to increase the number of the SDOF model control parameters: (1) to use it piecewise, or (2) to allow the three



parameters to vary. Reynolds and Soedel [7] used the first strategy by dividing the frequency range between 20 and 500 Hz into two regions, corresponding to high and low frequencies. The second strategy is to take restoring and dissipative coefficients dependent on the HAS vibration influencing factors. This strategy gives a more realistic model than the one with constant parameters. In this framework, Gurram et al. [13, 14], Marcotte et al. [15] and Aldien et al. [5] used linear hand forces dependent dissipative and restoring elements in their 3 and 4 DOF models. More recently, Hida et al. [16] used univariate Padé approximants and the nonlinear vibration transmissibility at the wrist, to identify the damping ratio and the stiffness coefficients in terms of the grip force or the excitation frequency.

The scope of this work is to use a SDOF mass-spring-damper nonlinear model that reproduces with high accuracy the experimentally measured DPMT or transmissibility of the human hand-arm system. To this effect, the mechanical elements of this model are taken active and depended on the influencing factors of the HAS biodynamic behavior. This dependence is expressed in terms of pole free multivariate Padé approximants [17, 18]. The model parameters identification is obtained by minimizing two independent constrained objective functions comprising real and imaginary parts of data errors or the transmissibility between the computed and measured DPMT. The main objective is to express the variation of the stiffness and the damping coefficients in terms of the influencing factors of the HAS vibration. To be noted that the restoring and dissipative parameters are not directly experimentally measurable and are not known for sure. In this framework, Rakheja et al. [10], obtained by analyzing 12 linear HAS models, that the computed stiffness coefficients lead to unrealistically high static deflections under 50N constant feed force. In addition, they found that the computed damping ratios ranged from 0.05 to 1060.28 in the Z-direction vibrations.

In the present work, the harmonic balance method [19] is used to derive analytical expressions of the nonlinear transmissibility and the DPMT. Using the proposed workflow, our models reproduce accurately the experimental measurements while varying more than one control parameter. More importantly, the proposed models lead to realistic stiffness and damping coefficients.

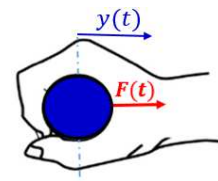
The present paper is organized as follows: in section 2, the mathematical models, the nonlinear transmissibility and DPMT, and the parameters identification workflow are presented. In section 3, the derived models are applied to three Z-direction HAS vibration measurement data. Lastly, the conclusion section concludes the paper by discussing the results and future directions.

2. Mathematical models and methods

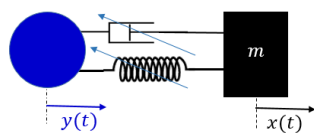
Figure 1 shows the HAS with Z-direction vibration in the case of extended posture with 180° elbow angle. Two single DOF biomechanical nonlinear models with one driving point are shown in Fig. 1c and Fig. 1d. The effect of the handle, drawn in blue, is taken as an imposed displacement in Fig. 1c, and as an external forcing in Fig. 1d. Figure 1e displays a 5 DOF model of the HAS with two driving points and the nonlinearity is assumed localized in the fingers. This model will be investigated elsewhere.



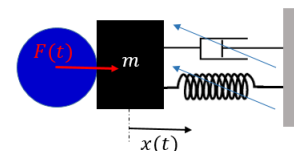
(a) The extended arm posture with 180° elbow angle



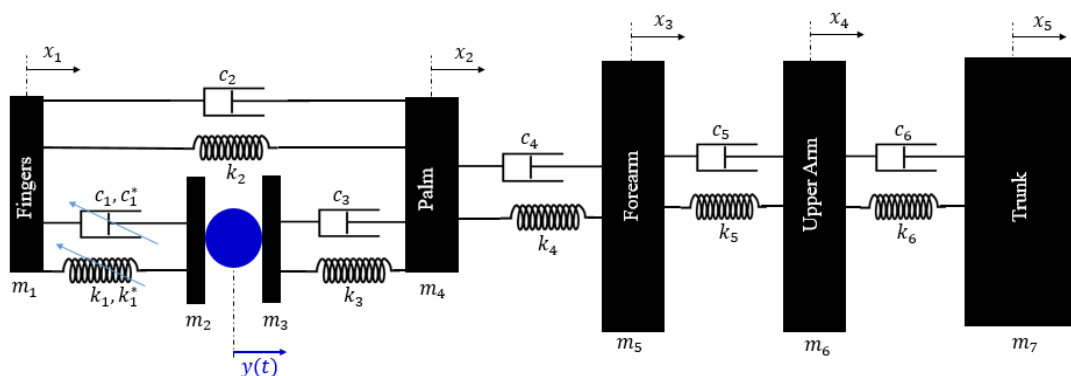
(b) Illustration of the arm-handle contact



(c) Single DOF in the case of an imposed displacement



(d) Single DOF in the case of an external forcing



(e) Five DOF model of the HAS with two driving points

Fig. 1. Mathematical models of the HAS in the case of Z-direction vibrations. The blue disk is the handle



The general equation of motion of single DOF models of the HAS, shown in Fig. 1c and Fig. 1d, can be written in a general framework as follows

$$m \ddot{x} + G(x(t), \dot{x}(t), t, \mu) = 0 \quad (1)$$

where m is the overall mass of the HAS, and $G(\cdot)$ is a polynomial function of the absolute displacement $x(t)$ and velocity $\dot{x}(t)$. Dots are derivatives with respect to time t and μ is the control parameters vector. Moreover, in our case $G(\cdot)$ contains explicit harmonic temporal terms with a frequency Ω . Then, the harmonic balance method (HBM) [19] is used to seek periodic solutions of Eq. (1) with a fundamental frequency equal to Ω , such that

$$x(t) = X \cos(\Omega t - \theta) + \text{h.o.t.} \quad (2)$$

where X and θ are the amplitude and the phase of the absolute displacement of the mass, respectively. The contribution of higher order harmonics terms (h.o.t) is assumed negligible. In all applications the function $G(\cdot)$ is assumed odd with respect to $x(t)$ and $\dot{x}(t)$.

2.1 Displacement transmissibility

The equation of motion of the HAS model shown in Fig.1(c) is given by

$$m \ddot{x} + c(\dot{x} - \dot{y}) + k(x - y) + c^* (\dot{x} - \dot{y})^3 + k^* (x - y)^3 = 0 \quad (3)$$

where k and c are the linear stiffness and viscous damping coefficients, respectively. The corresponding nonlinear coefficients are denoted k^* and c^* . The imposed harmonic displacement of the handle is denoted $y(t) = Y \cos(\Omega t)$, where Y and Ω are its amplitude and frequency, respectively.

Using the harmonic balance method, a first order approximation of the periodic solution of Eq. (3) is given by Eq. (2), where the amplitude X and the phase θ are given by

$$X = \sqrt{Y^2 + \frac{a^2}{2m\Omega^2} (3k^* a^2 + 4k - 2m\Omega^2)} \quad (4a)$$

$$\theta = \tan^{-1} \left(\frac{a \sin(\phi)}{a \cos(\phi) + Y} \right) \quad (4b)$$

with a and ϕ are the relative displacement amplitude and phase of the mass, respectively. The amplitude a is solution of the following sixth order algebraic equation

$$\frac{9}{16} (\Omega^6 c^{*2} + k^{*2}) a^6 + \frac{3}{2} (k^* (k - m\Omega^2) + c^* c^* \Omega^4) a^4 + ((k - m\Omega^2)^2 + c^2 \Omega^2) a^2 - m^2 Y^2 \Omega^4 = 0 \quad (5)$$

The phase ϕ of the relative displacement is given by

$$\phi = \tan^{-1} \left(\frac{3c^* \Omega^3 a^2 + 4c\Omega}{3k^* a^2 + 4k - 4m\Omega^2} \right) \quad (6)$$

The nonlinear parameters k^* and c^* appear in the fourth and the sixth polynomial terms in Eq. (5). Consequently, the relative amplitude a can have at most three real solutions.

The nonlinear displacement transmissibility is given by

$$T = \frac{X}{Y} = \sqrt{1 + \frac{a^2}{Y^2} + 2 \frac{a}{Y} \cos(\phi)} = \sqrt{1 + \frac{a^2}{Y^2} \left(\frac{3k^* a^2 + 4k - 2m\Omega^2}{2m\Omega^2} \right)} \quad (7)$$

The linear case is obtained by cancelling the effects of nonlinearities i.e., setting $k^* = c^* = 0$ in Eq. (5). Hence, the amplitude a_L of the relative displacement and the transmissibility T_L in the linear case are given by

$$a_L = \frac{m Y \Omega^2}{\sqrt{(k - m\Omega^2)^2 + c^2 \Omega^2}} \quad (8a)$$

$$T_L = \sqrt{\frac{k^2 + c^2 \Omega^2}{(k - m\Omega^2)^2 + c^2 \Omega^2}} \quad (8b)$$

To be pointed out that the linear transmissibility (8b) is independent of the imposed handle motion amplitude Y , whereas the nonlinear transmissibility (7) depends on it.

Based on vibration measurements on the HAS, Adewusi et al. [3] found experimentally, using two different magnitudes of broad-band random vibrations of handle, that the excitation magnitude affects the transmissibility, especially around the characteristic frequencies.

2.2 Driving-point mechanical impedance (DPMI)

The equation of motion of the HAS model shown in Fig.1(d) is given by

$$m \ddot{x} + c \dot{x} + kx + c^* \dot{x}^3 + k^* x^3 = F \cos(\Omega t) \quad (9)$$



The solution of Eq.(9) is sought in the form (2). Using the HBM, the amplitude X is solution of the following sixth algebraic order equation

$$\frac{9}{16}(\Omega^6 c^2 + k^2) X^6 + \frac{3}{2}(k^* (k - m\Omega^2) + c^* \Omega^4) X^4 + ((k - m\Omega^2)^2 + c^2 \Omega^2) X^2 = F^2 \quad (10a)$$

$$\theta = \tan^{-1} \left(\frac{3c^* \Omega^2 X^2 + 4c\Omega}{3k^* X^2 + 4k - 4m\Omega^2} \right) \quad (10b)$$

The force amplitude F should be measured in order to determine the displacement amplitude X by solving Eq.(10a). The DPMI Z is defined as the ratio of the dynamic force exerted on the mass and its velocity $\dot{x}(t)$. It is expressed in the frequency space, using the Fourier transforms $\Im(\cdot)$, as follows

$$Z = \frac{\Im(F \cos(\Omega t))}{\Im(\dot{x}(t))} = Z_r + j Z_{im} \quad (11)$$

where $j = \sqrt{-1}$, Z_r and Z_{im} are the real and imaginary parts of the DPMI, respectively. They are given by

$$Z_r = c - 3\pi^2 c^* f^2 X^2 ; \quad Z_{im} = 2\pi f m - \frac{k}{2\pi f} - \frac{3}{8\pi} \frac{k^*}{f} X^2 \quad (12)$$

The two parts of the nonlinear DPMI depend explicitly on the excitation frequency $f = \Omega/2\pi$ and the displacement amplitude X . Furthermore, the DPMI real part Z_r depends on the linear and the nonlinear damping coefficients c and c^* . The DPMI imaginary part Z_{im} depends on the mass m , the linear and the nonlinear stiffness coefficients k and k^* . To be noted that the real and imaginary parts of the DPMI can be computed independently.

The linear case is obtained by setting $k^* = c^* = 0$ in Eq. (12). Furthermore, the DPMI can also be expressed using its modulus $|Z|$ and its phase φ . In the case of a sinusoidal excitation, the vibration power absorption φ_{abs} into the HAS is expressed in terms of the real part of the DPMI and the handle velocity v_h [5, 6]. It is defined in the frequency space as follows

$$\varphi_{abs} = Z_r |v_h|^2 \quad (13)$$

The power absorption is used for assessing the risk and the damaging effects of vibration to the human HAS [6, 20].

2.3 Parameters identification

The majority of the HAS vibrations experiments, reported in the literature, vary only one single parameter at once. The mostly investigated parameters of control are the excitation frequency, followed by the grip and/or the push forces [9-11]. The parameters influencing the HAS biodynamic response are gathered in the control parameters r -vector $\mu = (\mu_1, \dots, \mu_r)$. This vector includes factors like the forcing properties, the grip and the push-pull forces, the anthropometric characteristics, etc.

In this work, the mass m is assumed constant, the linear stiffness k and the damping c coefficients, are expressed in terms of the vector μ , using the following multivariate Padé approximants of order $[M_k/N_k]$ and $[M_c/N_c]$, respectively

$$k(\mu) = \frac{\wp^{M_k}(\mu_1, \mu_2, \dots, \mu_r)}{1 + \wp^{N_k}(\mu_1, \mu_2, \dots, \mu_r)} \quad (14)$$

$$c(\mu) = \frac{\wp^{M_c}(\mu_1, \mu_2, \dots, \mu_r)}{1 + \wp^{N_c}(\mu_1, \mu_2, \dots, \mu_r)} \quad (15)$$

where $\wp^\alpha(\cdot)$ is an α order multivariate polynomial function of its arguments. To be noted that the polynomials in the numerator and the denominator can be dense or sparse.

The choice of the multivariate Padé approximants, instead of the widely used polynomial interpolants, is motivated by its performances in fitting data using fewer parameters. Moreover, high order polynomials are required to fit satisfactorily experimental data, leading to wild oscillatory models with poor extrapolation and/or interpolation results [17]. However, fractional functions suffer from the existence of poles corresponding to zeros of the denominator. In what follows, parameters causing poles, in the domain of interest, are excluded. In this work, minimum orders of the rational approximants (14) and (15) are sought in order to reduce the complexity of the interpolant. In fact, the polynomials in the numerator and the denominator are gradually increased and iteratively all combinations of powers are tested until the best accuracy is obtained. Furthermore, in order to ensure that the obtained results are realistic and interpolate reasonably, for all parameters of control, various realistic physical constraints are imposed on this multi-objective optimization problem. Hence, the mass, the stiffness and the damping coefficients are subjects to the following parametric constraints:

$$\forall \mu: \quad 3.5 < m < 6 \text{ Kg}; \quad k(\mu) > 1000 \text{ N/m}; \quad 0 < c(\mu) < 500 \text{ N.s/m} \quad (16)$$

The model constraints (16) are based on previously published works [10, 13]. The constraint of the linear stiffness coefficient is chosen also to lead to realistic deflections under static feed forces.

Unknown parameters of the model are identified by minimizing the overall distance between the theoretical and experimental DPMI or transmissibility respecting the imposed constraints (16). In the present work, a nonlinear fit least-squares error algorithm that minimizes the sum of squares errors is used [21]. In fact, this minimization process is applied independently to the real and to the imaginary parts of the DPMI. The unknown parameters of the stiffness and the damping coefficients given in Eqs. (14) and (15) are varied iteratively, and the best results that respect the constraints (16) are reported.



In order to measure the outcomes quality of the fitting process, we use the correlation coefficient and the root-mean-square error (RMSE) between the theoretical Γ^{th} and the measured Γ^{ex} quantities. The RMSE is defined as

$$\text{RMSE} = \sqrt{\frac{1}{N} \sum_{n=1}^N (\Gamma^{\text{th}}(\mu_n) - \Gamma^{\text{ex}}(\mu_n))^2} \quad (17)$$

where N is the number of measurements and Γ can be $T, Z_r, Z_{im}, |Z|$ or φ .

3. Applications and discussions

In this section, the identification workflow of the stiffness and damping coefficients presented in the previous section is applied to three Z_h -direction HAS vibrations measurements. The first application is related to measurement data of transmissibility [9]. The second corresponds to the ISO-10068 (2012) limit DPMI values versus the excitation frequency; see [12, 13]. The third concerns the experimental DPMI data, in the case of imposing harmonic vibrations, while varying both the excitation frequency and the grip force [22, 23].

3.1 Transmissibility versus the grip force

Pan et al. [9] conducted a series of experiments for a hand-arm posture corresponding to bent-arm with 90° elbow angle. In the present paper, the wrist vibration transmissibility is investigated when varying the grip force F_g for four handle discrete sinusoidal vibrations with frequencies 10Hz, 16Hz, 25Hz and 40 Hz. They are used as imposed displacement on a cylindrical handle with a constant velocity of 0.1 m/s.

In this example, only the linear stiffness coefficient is developed as a $[4/2]$ order sparse fractional function in terms of the grip force, the other coefficients are taken constant.

$$k(F_g) = \frac{\sum_{n=0}^4 \kappa_n F_g^n}{1 + \beta_2 F_g^2} \quad (18)$$

Figure 2 shows the displacement transmissibility at the wrist versus the grip force for various excitation frequencies when using the nonlinear transmissibility displacement given in Eq. (7). This figure shows the good agreements between the nonlinear model and the experimental measurements. Figure 3 shows the predicted displacement amplitude of the wrist versus the grip force. It shows that the amplitude is decreasing with increasing the handle frequency. Figure 4 displays the predicted damping ratio versus the grip force. This ratio is decreasing with increasing the excitation frequency and the grip force.

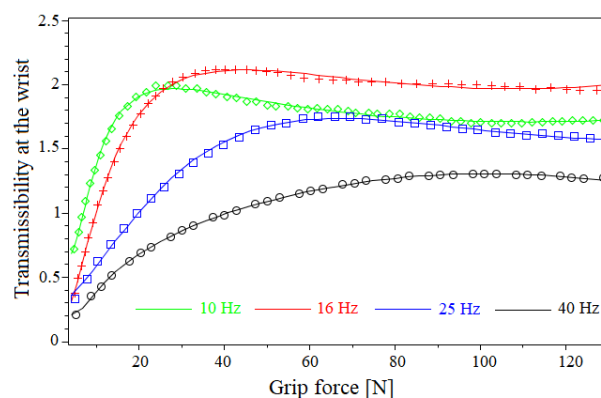


Fig. 2. Displacement transmissibility at the wrist versus the grip force for various excitation frequencies. Lines correspond to the computed transmissibility. The measured data [9] are shown in symbols

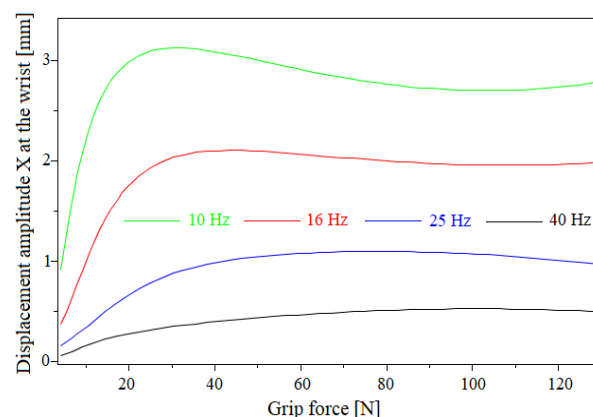


Fig. 3. Predicted displacement amplitude X at the wrist versus the grip force for various excitation frequencies.



Table 1. RMSE and correlations, of various DPMI quantities, between the measured data and the results of our model

	Z_r [N.s/m]		Z_{sm} [N.s/m]		$ Z $ [N.s/m]		φ [degrees]	
	RMSE	Corr	RMSE	Corr	RMSE	Corr	RMSE	Corr
Lower limit	0.90	0.999	2.47	0.997	1.23	0.998	1.16	0.997
Upper limit	1.20	0.999	2.16	0.999	1.51	0.999	0.34	0.998

3.2 DPMI versus frequency

The workflow is applied to the synthesized DPMI data presented in [20] as the most probable range of the driving point mechanical impedance phase and magnitude of the HAS. These data sets contain, in the three hand directions, the lower and the upper limits of the accepted modulus and phase of the DPMI values versus the frequency of excitation. Moreover, these data were adopted by the ISO-10068 (2012).

In this work, only the Z-direction DPMI is investigated in terms of the excitation frequency. The data set contains 24 one-third octave frequency bands measurements in the frequency range of 10 to 500 Hz, see [20]. Hence, the stiffness k and the damping c coefficients are expressed as functions of the frequency f as follows

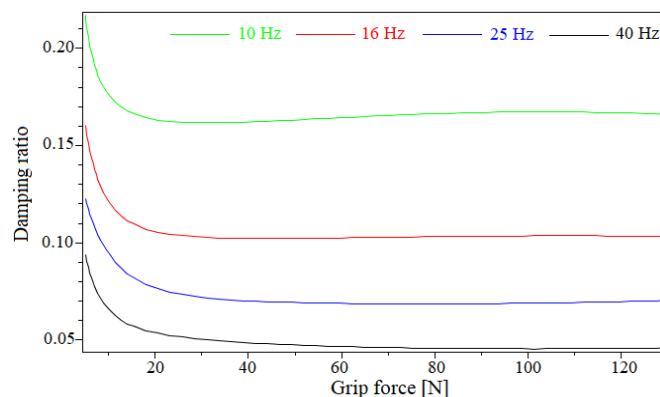
$$k(f) = \frac{\sum_{n=0}^M \kappa_n f^n}{1 + \sum_{n=0}^N \beta_n f^n} \quad c(f) = \frac{\sum_{n=0}^M c_n f^n}{1 + \sum_{n=0}^N \sigma_n f^n} \quad (19)$$

The dependency on the excitation frequency, of restoring and dissipative parameters, is a realistic way to model the visco-elastic properties of the skin-muscle-bone system composing the HAS. All combinations of the univariate Padé approximants powers up to order $[M = 5 / N = 5]$ are tested. Then, the best fitting theoretical model, which leads to the minimal error function, is selected. Hence, the fractional polynomials of order $[4/3]$ and $[5/3]$ are selected for the stiffness and the damping coefficients, respectively. In Table 1 are given the root-mean-square errors (RMSE) and the correlation coefficients (Corr), between the measured data and our models results, for various quantities of the DPMI. Table 1 reveals the excellent agreement between the results of our model and the measured data. In fact, all correlation coefficients are higher than 0.99 and all RMSE are below 2.5.

Figure 5 shows comparisons of Z-direction DPMI modulus and phase, of the theoretical model and the ISO data, versus the excitation frequency in the range [10 Hz, 500 Hz]. The computed results are drawn in continuous line while the lower and the upper bounds given in the ISO-10068 (2012) are presented in circles.

Figure 6a shows that the stiffness coefficient k of the HAS model increases with increasing the excitation frequency and it ranges in the mega-Newton per meter [MN/m] for high frequencies. This range is in agreement with the experimental results obtained by Singh et al. [21] when investigating experimentally human male elbow bones. They found that the mean compression stiffnesses of Humerus, Ulna and Radius are 16, 12 and 9 [MN/m], respectively. Furthermore, the stiffness coefficient of the lower bound is higher than the stiffness of the upper bound of the DPMI modulus. Figure 6b shows that the damping ratio of the HAS is decreasing with increasing the excitation frequency. The upper bound has a higher damping ratio than the lower bound for frequencies lower than 80 Hz. Above this frequency the two bounds have almost the same damping ratio that tends to zero asymptotically. Figures 6a and 6b suggest that soft tissues, which contain skin and subcutaneous tissues, of the HAS are excited for low frequencies since the stiffness is low and the damping ratio is high. In fact, bones are excited for high frequencies since their stiffness is high and their damping ratio is low. More importantly, the stiffness coefficient and the damping ratio displayed in Figure 6 can be viewed as the upper and the lower limits, in the frequency interval [10, 500 Hz] and in the Z direction, of the overall stiffness coefficient and damping ratio for the human hand arm system. In addition, these curves can also be used as lower and upper envelopes for the constraints to be imposed, on the overall stiffness coefficient and damping ratio, in the process of optimization and identification of the parameters of theoretical models.

In Fig. 7 are displayed the computed static deflections, of the upper and the lower bounds, under 50 N steady feed force in the excitation frequency range [10 Hz, 50 Hz]. This deflection is decreasing with increasing the frequency. Moreover, the deflection difference between the upper and the lower bounds is decreasing with increasing the frequency. In fact, the upper bound has a lower stiffness than the lower bound, consequently it has higher deflection. Figure 8 gives the computed upper and the lower limits of the maximum static deflection, in the Z-direction, versus the static feed deflection. It shows that this maximum deflection is in millimeter ranges, corresponding to the excitation frequency 10 Hz, and that it increases linearly with the increase of the static feed force. Furthermore, these limits can be used as constraints in the optimization process and in the parameter's identification.

**Fig. 4.** Predicted damping ratio versus the grip force for various handle frequencies.

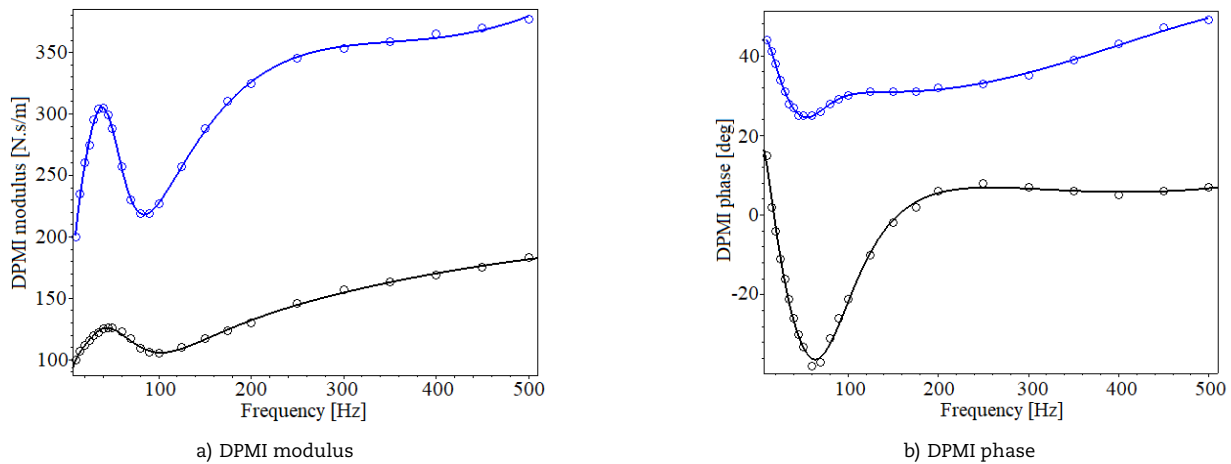


Fig. 5. Comparisons of Z-direction DPMI modulus and phase versus the excitation frequency. Circles are ISO-10068(2012). The theoretical results: upper bound in blue and lower bound in black.

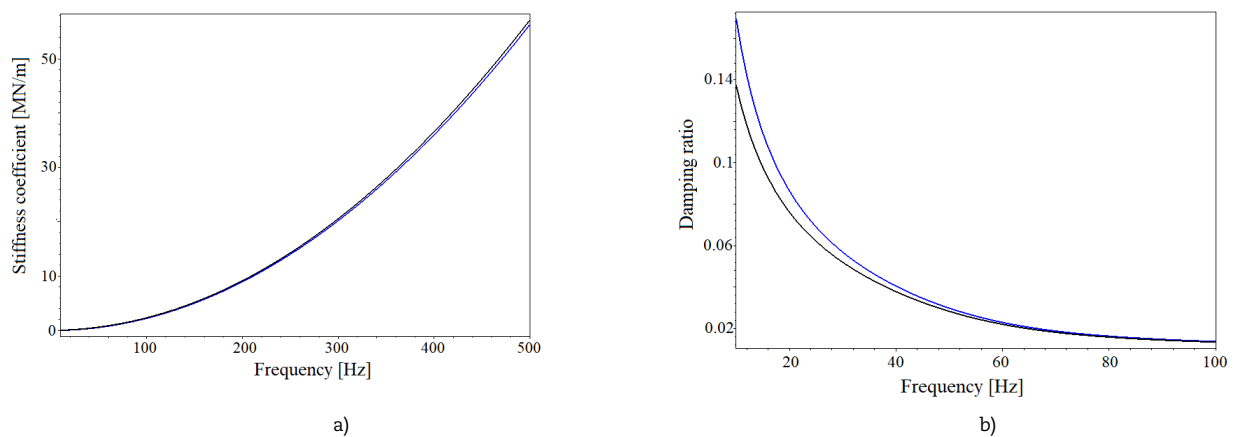


Fig. 6. Stiffness coefficient and the damping ratio versus the excitation frequency. The upper bound in blue and the lower bound in black.

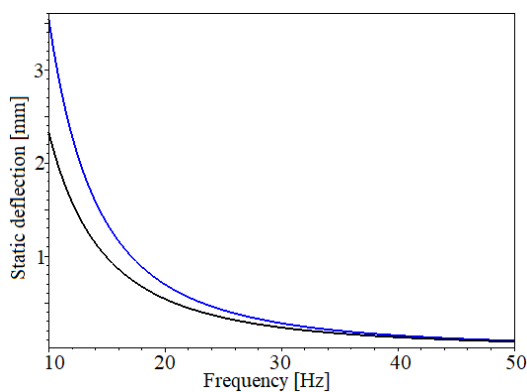


Fig. 7. Static deflection versus the excitation frequency under 50 N feed force. The upper bound in blue and the lower bound in black.

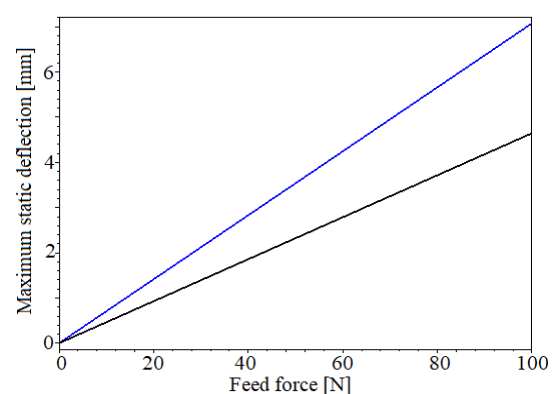


Fig. 8. Maximum static deflection versus the feed force for 10 Hz excitation frequency. The upper bound in blue and the lower bound in black.

3.3 DPMI versus the excitation frequency and the grip force

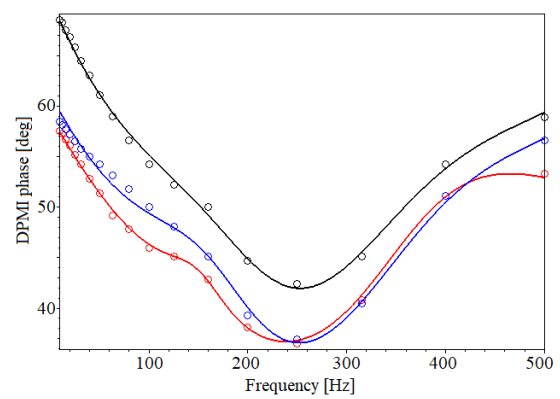
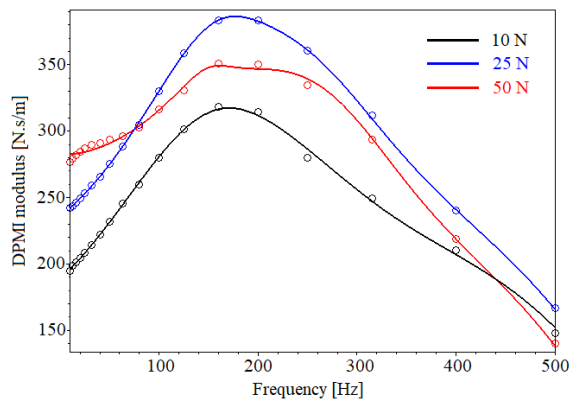
Gurram et al. [22, 23] conducted a series of experiments to measure DPMI in the three hands directions. These experiments were conducted, using a 38 mm diameter handle, at three different grip force levels of 10 N, 25 N and 50 N under sinusoidal imposed vibrations having three constant acceleration amplitudes of g , $2g$ and $3g$. The arm was maintained in a horizontal position with the elbow bent 90 degrees. The excitation frequency f and the grip force F_g are varied during this experiment. The 54 experimental data of the Z-direction DPMI are listed in [22].

In what follows, the mass of the HAS will be taken constant and equal to 5.8 kg. This value is the mass determined, in the previous application, for Z-direction data of the ISO-10068 (2012). The stiffness and the damping coefficients are expressed as multivariate Padé approximants function of the excitation frequency f and the grip force F_g , as follows

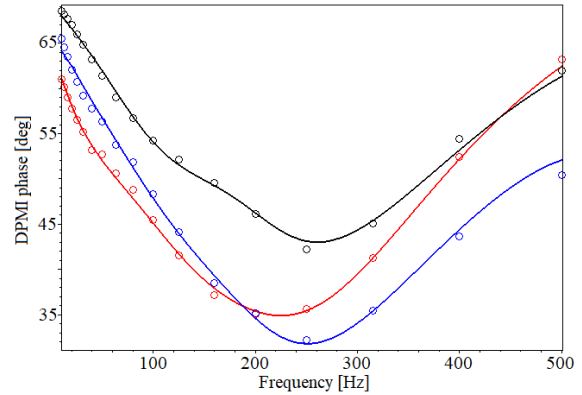
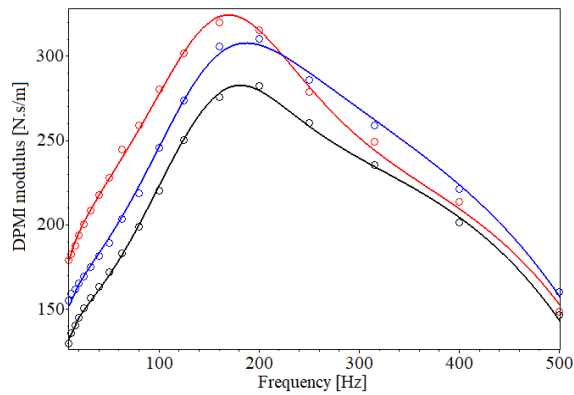


Table 2. Identified parameters of the damping and stiffness coefficients, for 2g amplitude

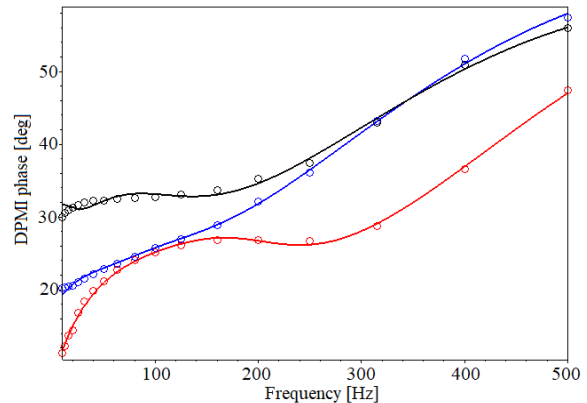
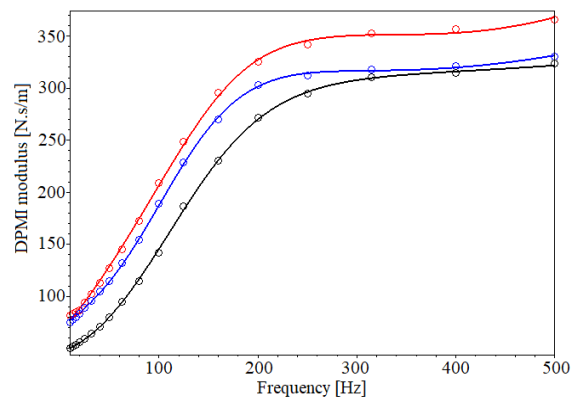
Damping coefficient parameters			
$c_{0,0} = 228.4$	$c_{1,1} = 55560.9538$	$c_{1,2} = 1278.1341$	$c_{1,0} = 254548.9576$
$c_{0,1} = -15016.1727$	$c_{2,1} = 52.2810$	$c_{2,0} = -3751.2992$	$c_{0,2} = 69339.8850$
$c_{1,3} = -30.0261$	$c_{3,0} = 124.6218$	$c_{0,3} = 4018.8253$	$c_{2,2} = -9.8503$
$c_{4,0} = -0.2034$	$c_{0,4} = -101.2559$	$c_{3,1} = 0.7720$	$\sigma_{1,0} = 13610.9124$
$\sigma_{0,1} = -5117.8455$	$\sigma_{1,1} = -285.1447$	$\sigma_{2,0} = -41.0324$	$\sigma_{0,2} = 3924.9845$
$\sigma_{1,2} = 2.4519$	$\sigma_{3,0} = 0.4293$	$\sigma_{0,3} = -69.8261$	$\sigma_{2,1} = -0.8906$
Stiffness coefficient parameters			
$\kappa_{0,0} = 1000.1$	$\kappa_{2,0} = 235.1985$	$\kappa_{3,0} = -2.0058$	$\kappa_{4,0} = 0.0054$
$\kappa_{5,0} = -0.0000006$	$\kappa_{1,1} = -137.1256$	$\kappa_{1,2} = 5.5754$	$\kappa_{1,3} = -0.0653$
$\kappa_{3,1} = 0.0065$	$\kappa_{2,1} = 0.1243$	$\kappa_{2,2} = -0.0017$	$\beta_{1,0} = -0.0086$
$\beta_{2,0} = 0.00002$	$\beta_{0,1} = 0.0003$	$\beta_{1,1} = 0.00003$	$\beta_{0,2} = -0.000005$



Case of g acceleration amplitude



Case of 2g acceleration amplitude



Case of 3g acceleration amplitude

Fig. 9. DPMI modulus and phase versus the excitation frequency, for 10N, 25N and 50N grip forces. Experimental data [18] in circles and theoretical results in lines

Table 3. RMSE and the correlation of various quantities of DPPI, for 2g amplitude

	RMSE	Correlation
Z_r [N.s/m]	2.30	0.999
Z_{im} [N.s/m]	2.29	0.995
$ Z $ [N.s/m]	2.45	0.999
φ [degrees]	0.59	0.998

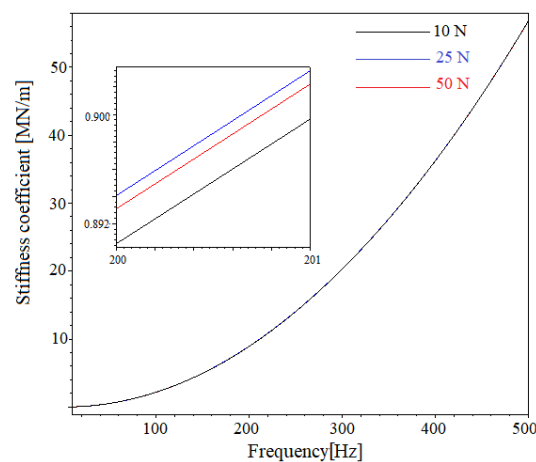
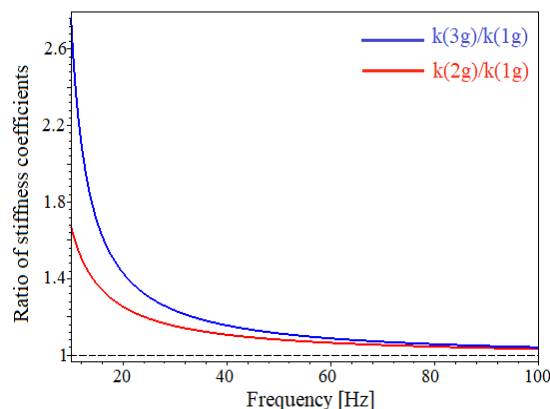
$$k(f, F_g) = \frac{\sum_{i+n=0}^{i+n=M} \kappa_{i,n} f^i F_g^n}{1 + \sum_{i+n=0}^{i+n=N} \beta_{i,n} f^i F_g^n} \quad c(f, F_g) = \frac{\sum_{i+n=0}^{i+n=M} c_{i,n} f^i F_g^n}{1 + \sum_{i+n=0}^{i+n=N} \sigma_{i,n} f^i F_g^n} \quad (20)$$

The identified parameters are listed in Table 2 in the case of 2g acceleration amplitude. Table 3 gives the root-mean-square errors (RMSE) and the correlation coefficient between the experimental and the theoretical DPPI. All correlations are above 0.99 and all RMSE are below 2.5, this proves the high accuracy and the validity of the theoretical model.

Figure 9 illustrates comparisons of the theoretical and the experimental DPPI modulus and phase in the case of g , $2g$ and $3g$ acceleration amplitude of the handle. Three grip forces are considered that are 10N, 25N and 50N. These plots show the agreement between the experimental data [22], in circles, and the theoretical model in continuous lines.

Figure 10 shows the variation of the derived theoretical stiffness coefficient versus the excitation frequency for the three grip forces (10N, 25N and 50N), in the case of 2g excitation amplitude. This figure reveals that the stiffness increases with increasing the excitation frequency regardless of the grip force values. For high frequencies, values of the stiffness coefficient are in the range of mega Newton per meter. The same tendencies of the stiffness coefficient are obtained for the excitation acceleration amplitudes $1g$ and $3g$.

In Figure 11 are shown ratios of the stiffness coefficients of the excitation amplitudes $2g$ and $3g$ to the stiffness coefficient corresponding to g , in the case of 50 N grip force. These ratios are decreasing with increasing the excitation frequency and they tend to unity for high frequencies. This decreasing indicates that the overall stiffness coefficient of the HAS is becoming independent of the excitation acceleration amplitude for excitation frequencies beyond 100 Hz. Moreover, in low frequencies, Figure 11 reveals that increasing the acceleration amplitude of the handle increases the stiffness of the HAS in a nonlinear manner. This tendency in low frequencies can be explained by additional muscular contraction caused by the tonic vibration reflex [24].

**Fig. 10.** Stiffness coefficient versus the excitation frequency for various grip forces, in the case of 2g excitation amplitude**Fig. 11.** Ratios of stiffness coefficients versus the excitation frequency for 50 N grip force

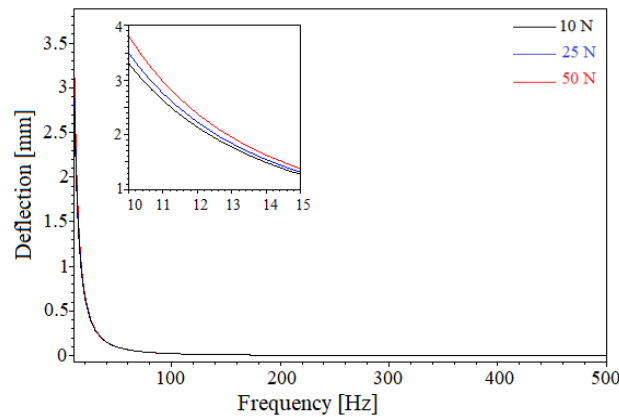


Fig. 12. Static deflection versus the excitation frequency for various grip forces, in the case of $2g$ excitation amplitude

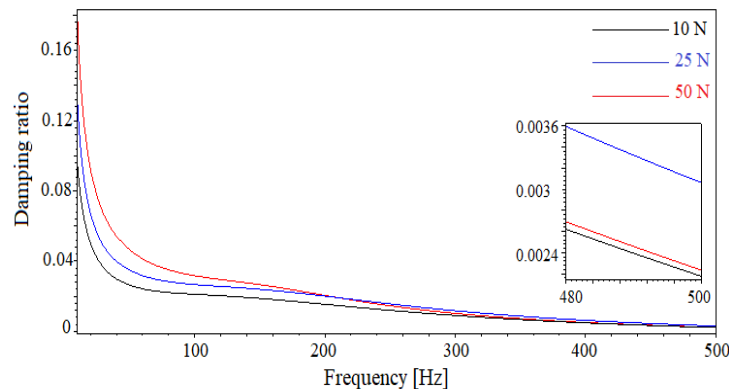


Fig. 13. Damping ratio, for $2g$ excitation amplitude, versus the excitation frequency for various grip forces

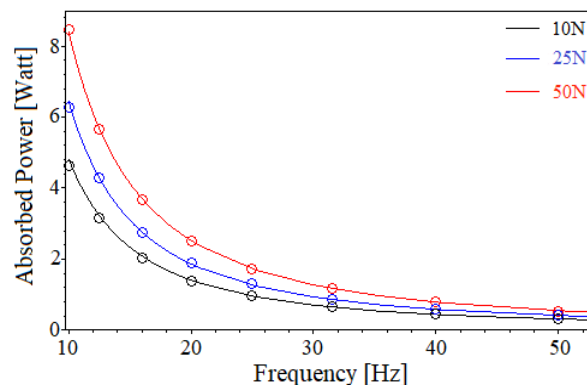


Fig. 14. Vibration power absorption spectra for various grip forces, in the case of $2g$ excitation amplitude. Circles denote the experimental measurements.

Figure 12 displays the static deflection of the driving point, under a constant feed force of 50 N, versus the excitation frequency for the three grip forces. Figure 12 demonstrates that the static deflection is decreasing with increasing the frequency, regardless of the grip force. Furthermore, in low frequencies, increasing the grip force induces higher static deflection. In high frequencies, the effect of the grip force is negligible and the static deflection tends to zero. For the same data sets that we are using, Rakheja et al. [10] computed the static deflection; under 50N feed force, of a 3-DOF and a 4-DOF models. They found unrealistic constant static deflections of 566.2 mm for the 3-DOF model and 571.5 mm for the 4-DOF model. As reported in the magnification of Figure 11, the maximum static deflection computed by our model is less than 4 mm for the three used grip forces. Our results are realistic since the static deflection of the skin and tissues in the human hand, in contact with the handle, are relatively low.

Figure 13 displays the derived damping ratio versus the excitation frequency for the three grip forces (10N, 25N and 50N) in the case of $2g$ acceleration amplitude. It reveals that the derived damping ratio is decreasing to increasing the excitation frequency for the three values of the grip force. The decrease rate is bigger for low frequencies (< 40 Hz). In addition, the damping ratio is less than 0.18 for all three grip forces. For the same Z-axis experimental measurements, Rakheja et al. [10] found the following constant damping ratios: (2.36, 42.31, 0.10) for the 3-DOF model and (2.94, 3.52, 15.44, 0.23) for the 4-DOF model. They concluded that the models with high damping ratios and low stiffness coefficients are not adequate for the realization of a mechanical hand-arm simulator. To be noted that the damping ratio is behaving similarly for the accelerations levels $1g$ and $3g$.

Figure 14 illustrates comparisons of the measured and theoretical vibration power absorption spectra, in the case of $2g$ excitation amplitude, for 10N, 25N and 50N grip forces. These spectra reveal that the power absorption of the HAS is predominant in the low-frequency range [10 Hz, 30 Hz] and it is decreasing with increasing the excitation frequency.



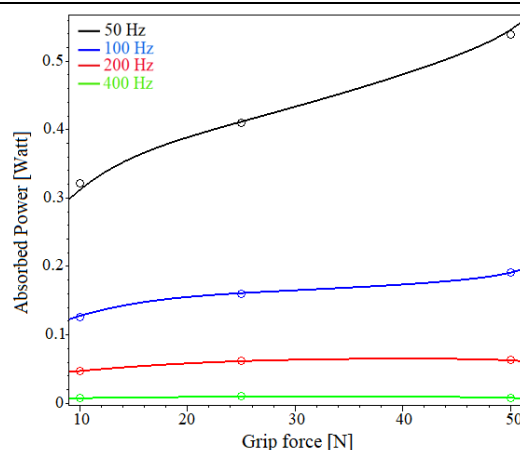


Fig. 15. Vibration power absorption versus the grip force, for various excitation frequencies, in the case of $2g$ acceleration amplitude. Circles denote the experimental measurements

Figure 15 shows the vibration power absorption of the HAS versus the grip force, in the case of $2g$ excitation amplitude, for various excitation frequencies. The experimentally measured power absorption in [22] is shown as circles. Figure 15 reveals that the grip force has a major influence on the absorbed power only at low frequencies where increasing the grip force increases the absorbed power.

4. Conclusion

This study aimed at the development of simple biodynamic models of the human hand-arm system (HAS) that enables among others the computation of the stiffness and the damping coefficients. The models consisted of two nonlinear single DOF system with the stiffness and the damping coefficients dependent on the HAS vibration influencing factors. These dependencies were expressed using multivariate Padé approximants. Using the harmonic balance method, expressions of the nonlinear displacement transmissibility and DPMI were derived. The model parameters were identified by minimizing constrained objective function errors between the computed and measured target transmissibility or DPMI characteristics. The proposed workflow was applied to three different Z-direction measured data. The stiffness coefficient and the damping ratio were computed in terms of the excitation frequency and/or the grip force. The proposed models can be utilized as a simulator of the HAS using Magneto-rheological dampers and variable stiffness materials. It is noteworthy that our single-DOF models give the overall biodynamic response of the HAS and are not able to give information about the response in the HAS subsystems. Our future research venues will focus on applying the same workflow to Multi-DOF linear and nonlinear models of the HAS, with varying parameters, in order to have more information on the distribution of the biodynamic responses of the HAS.

Author Contributions

N. Hida planned the scheme, initiated the project, and suggested the models and the simulations; M. Abid conducted the simulations and analyzed the empirical results; F. Lakrad developed the mathematical modeling and examined the theory validation. The manuscript was written through the contribution of all authors. All authors discussed the results, reviewed, and approved the final version of the manuscript.

Conflict of Interest

The authors declared no potential conflicts of interest with respect to the research, authorship, and publication of this article.

Funding

The authors received no financial support for the research, authorship, and publication of this article.

References


- [1] Griffin, M.J., *Handbook of human vibration*, Academic Press, London, 1996.
- [2] Mansfield, N.J., *Human response to vibration*, CRC Press, 2004.
- [3] Adewusi, S.A., Rakheja, S., Marcotte, P., Boutin, J., Vibration transmissibility characteristics of the human hand-arm system under different postures, hand forces and excitation levels, *Journal of Sound and Vibration*, 329, 2010, 2953-2971.
- [4] Saha, S., Kalra, P., A review on hand-arm vibration exposure and vibration transmissibility from power hand tools to hand-arm system, *International Journal of Human Factors and Ergonomics*, 4(1), 2016, 10-46.
- [5] Aldien, Y., Marcotte, P., Rakheja, S., Boileau, P.E., Influence of hand forces and handle size on power absorption of the human hand-arm exposed to z-h axis vibration, *Journal of Sound and Vibration*, 290, 2006, 1015-1039.
- [6] Dong, J.H., Dong, R.G., Rakheja, S., Welcome, D.E., McDowell, T.W., Wu, J.Z., A method for analyzing absorbed power distribution in the hand and arm substructures when operating vibrating tools, *Journal of Sound and Vibration*, 311, 2008, 1286-1304.
- [7] Reynolds, D.D., Soedel, W., Dynamic response of the hand-arm system to a sinusoidal input, *Journal of Sound and Vibration*, 21(3), 1972, 339-353.
- [8] Lundström, R., Burström, L., Mechanical impedance of the human hand-arm system, *International Journal of Industrial Ergonomics*, 3, 1989, 235-342.
- [9] Pan, D., Xu, X.S., Welcome, D.E., McDowell, T.W., Warren, Ch., Wu, J., Dong, R.G., The relationships between hand coupling force and vibration biodynamic responses of the hand-arm system, *Ergonomics*, 6(16), 2018, 818-830.
- [10] Rakheja, S., Wu, J.Z., Dong, R.G., Schopper, A.W., Boileau, P.E., A comparison of biodynamic models of the human hand-arm system for applications to hand-held power tools, *Journal of Sound and Vibration*, 249(1), 2002, 55-82.
- [11] Dong, R.G., Dong, J.H., Wu, J.Z., Rakheja, S., Modeling of biodynamic responses distributed at the fingers and the palm of the human hand-arm system, *Journal of Biomechanics*, 40, 2007, 2335-2340.
- [12] ISO-10068, Mechanical vibration and shock, mechanical impedance of the human hand-arm system at the driving point, *International*





Organization for Standardization, Geneva, Switzerland, 2012.

- [13] Gurram, R., Rakheja, S., Brammer, A.J., Driving-point mechanical impedance of the human hand-arm system: Synthesis and model development, *Journal of Sound and Vibration*, 180, 1995, 437-458.
- [14] Gurram, R., Rakheja, S., Boileau, P.E., Gouw, G.J., Development of a grip force dependent hand-arm vibration model, *Central European Journal of Public Health*, 4(1), 1996, 65-68.
- [15] Marcotte, P., Aldien, Y., Boileau, P.E., Rakheja, S., Boutin, J., Effect of handle size and hand-handle contact force on the biodynamic response of the hand-arm system under zh-axis vibration, *Journal of Sound and Vibration*, 283, 2005, 1071-1091.
- [16] Hida, N., Abid, M., Lakrad, F., A nonlinear model of the hand-arm system and parameters identification using vibration transmissibility, *MATEC Web of Conferences*, 241, 2018, 01014.
- [17] Braess, D., *Nonlinear approximation theory*, Springer-Verlag, Berlin, 1986.
- [18] Guillaume, P., Huard, A., Multivariate Padé approximation, *Journal of Computational and Applied Mathematics*, 121(1-2), 2000, 197-219.
- [19] Nayfeh, A.H., *Introduction to perturbation methods*, John Wiley and Sons, New-York, 1981.
- [20] Burström, L., Measurement of the mechanical energy absorption in the hand and arm whilst using vibrating tools, *Journal of Low Frequency Noise and Vibration*, 9(1), 1990, 1-14.
- [21] Bates, D.M., Watts, D.G., *Nonlinear regression and its applications*, Wiley, New York, 1988
- [22] Gurram, R., A study of vibration response characteristics of the human hand-arm system, Ph.D. Thesis, Department of Mechanical Engineering, Concordia University, Montreal, Quebec, 1993.
- [23] Gurram, R., Rakheja, S., Gouw, G.J., Mechanical impedance of the human hand-arm system subject to sinusoidal and stochastic excitations, *International Journal of Industrial Ergonomics*, 16, 1995, 135-145.
- [24] Kefauver, J.M., Ward, A.B., Discoveries in structure and physiology of mechanically activated ion channels, *Nature*, 587, 2020, 567-576.
- [25] Yildirim, M.A., Topkara, B., Aydin, T., Parker, N., Soy, D., Coskun, E., Ones, K., Bardak, A., Kesiktaş, N., Ozyurt, M.G., Celik, B., Onder, B., Kilic, Aysegul, Kucuk, H.C., Karacan, Ilhan, Türker, K.S., Exploring the receptor origin of vibration-induced reflexes, *Spinal Cord*, 58, 2020, 716-723.

ORCID iD

Nahid Hida  <https://orcid.org/0000-0002-4142-5027>

Mohamed Abid  <https://orcid.org/0000-0001-9402-2822>

Faouzi Lakrad  <https://orcid.org/0000-0003-0392-0737>



© 2021 by the authors. Licensee SCU, Ahvaz, Iran. This article is an open access article distributed under the terms and conditions of the Creative Commons Attribution-NonCommercial 4.0 International (CC BY-NC 4.0 license) (<http://creativecommons.org/licenses/by-nc/4.0/>).

How to cite this article: Hida N., Abid M., Lakrad F. Nonlinear Biodynamic Models of the Hand-arm System and Parameters Identification using the Vibration Transmissibility or the Driving-point Mechanical Impedance, *J. Appl. Comput. Mech.*, 7(2), 2021, 944–955. <https://doi.org/10.22055/JACM.2021.35508.2672>

